Chapter 12
Phase Reconstruction with Iterated Hilbert Transforms

Erik Gengel and Arkady Pikovsky

Abstract We discuss theoretical and practical issues of data-driven phase reconstruction approaches for nonlinear oscillatory systems by means of the geometric technique of embeddings and protophase-to-phase transformation. In this chapter, we introduce a natural extension of the well-studied Hilbert transform by iteration. The novel approach, termed iterated Hilbert transform embeddings, implements central assumptions underlying phase reconstruction and allows for exact demodulation of purely phase modulated signals. Here, we examine the performance of the novel method for the more challenging situation of generic phase-amplitude modulated signals of a simple nonlinear oscillatory system. In particular we present the benefits of the approach for secondary phase analysis steps illustrated by reconstruction of the phase response curve. Limitations of the approach are disussed for a noise-driven phase dynamics.

E. Gengel · A. Pikovsky (✉)
Institute for Physics and Astronomy, Universit of Potsdam, Karl-Liebknecht-Str. 24/25, 14476 Potsdam, Germany
e-mail: pikovsky@uni-potsdam.de

E. Gengel
e-mail: egengel@uni-potsdam.de

E. Gengel
Friedrich-Ebert Stiftung, Bonn, Germany

A. Pikovsky
Higher School of Economics, Nizhny Novgorod, Russia

Department of Control Theory, Institute of Information Technologies, Mathematics and Mechanics, Lobachevsky University Nizhny Novgorod, Nizhny Novgorod, Russia

A. Stefanovska and P. V. E. McClintock (eds.), *Physics of Biological Oscillators*, Understanding Complex Systems,
https://doi.org/10.1007/978-3-030-59805-1_12

12.1 Introduction and Overview

This chapter deals with the art of phase reconstruction. We focus on Hilbert transforms, however, much of the introduced methodology is not bound to Hilbert transforms alone.

In general, three approaches to signal analysis of oscillatory signals can be identified. The first approach applies statistical methods to extract information from observations assuming no further model [2, 22, 34]. The second approach takes the theory of dynamical systems into account and analyses the signals in terms of the phase and the amplitude notions provided in this theory [1, 7, 9, 17–19, 24, 29, 30, 37]. In an intermediate methodology, a phase and an amplitude are extracted from the data and then analysed in terms of statistical quantities. These methods may or may not take an underlying theory into account [15, 23, 25, 28, 36, 42, 43] Alternatively, one applies machine learning techniques to obtain equations of motion directly from observations [6, 41].

Here we focus on signal analysis approaches suitable for oscillating systems. The basic assumption is that the signal originates from a dynamical oscillating system, interacting with other systems and/or with the environment, and the goal is to understand the dynamics. This task is especially important and challenging in life science, where a theoretic description of the oscillators is in many cases lacking, because the underlying mechanisms are not clear. On the other hand, measurements of the full phase space dynamics are impossible, or would destroy the system itself. The latter aspect introduces the common setting where measurements of the systems are passive, i.e., an observer collects data from the free running system and may only apply weak perturbations to prevent damage. For such passive observations, we pursue here the approach inspired by the dynamical system theory: we try to extract the phases from the signals, with the aim to build models as close to theoretical descriptions as possible.

The ideas of the phase dynamics reconstruction has been widely used in physics, chemistry, biology, medicine and other areas [4, 20, 31, 35] to understand properties of oscillators and coupling between them (see also Chaps. 2, 3 and 11 of this book). The reason for this, as we discuss below, is that the phase is sensitive to interactions and external perturbations. In particular, many studies apply Hilbert transforms to reconstruct the phase from data (for example see [3, 14, 38, 43] and references therein). However, several fundamental issues in the process of phase reconstruction are unresolved, long standing and mostly omitted in the community. One issue deals with the role of the amplitudes [8, 21]. And from the view point of pure signal processing: how to deal with phase-amplitude mixing in Hilbert transforms [10, 13]. The latter issue will be discussed in particular here and we describe a solution by virtue of *iterative Hilbert transform embeddings* (IHTE) [12].

First, we describe the theoretical concepts. We then discuss the art of phase reconstruction with a focus on IHTE. We illustrate this method by presenting results for a Stuart-Landau non-linear oscillator, including reconstruction of the *infinitesimal phase response curve* (iPRC). Finally, we discuss difficulties of application in case of noisy oscillations.

12.2 Nonlinear Oscillators and Phase Reduction

Here we briefly review the phase reduction of driven limit cycle oscillators, for more details see [26, 27]. An autonomous oscillator is described by N state variables $\mathbf{y}$ which evolve according to a system of differential equations $\dot{\mathbf{y}} = \mathbf{f}(\mathbf{y})$. One assumes that this system has a stable limit cycle $\mathbf{y}_0(t) = \mathbf{y}_0(t + T)$ describing periodic (period T) oscillations. In the basin of attraction of the cycle one can always introduce a phase variable φ which grows uniformly in time

$$\dot{\varphi} = \omega = \frac{2\pi}{T}. \tag{12.1}$$

On the limit cycle, only the phase varies, so that $\mathbf{y}_0(\varphi) = \mathbf{y}_0(\varphi + 2\pi)$, which means that the value of the phase uniquely determines the point on the limit cycle.

If the autonomous oscillator is perturbed, i.e., it is driven by a small external force $\dot{\mathbf{y}} = \mathbf{f}(\mathbf{y}) + \varepsilon\mathbf{p}(\mathbf{y}, t)$, then the system slightly (of order $\sim \varepsilon$) deviates from the limit cycle, and additionally the phase does not grow uniformly, but obeys (in the first order in ε) the equation

$$\dot{\varphi} = \omega + \varepsilon Q(\varphi, t), \tag{12.2}$$

where Q can be expressed via $\mathbf{f}$, $\mathbf{p}$ (see [26] for details). Equation (12.2) contains only the phase and not the amplitude, it can be viewed as a result of the *phase reduction*. The dynamics of the phase according to (12.2) allows for studying different important effects of synchronization, etc. In the case when the oscillator is forced by another one, the force $\mathbf{p}(\eta)$ can be viewed as a function of the phase $\eta(t)$ of this driving oscillator, so the function $Q(\varphi, \eta)$ becomes the coupling function depending on two phases. In experimental situations it is quite common to perturb just one variable of the system. In that case, if the forcing term is scalar and does not depend on the system variables, one can factorize $Q(\varphi, t) = Z(\varphi)P(t)$ into the iPRC $Z(\varphi)$ and the (scalar) external driving $P(t)$ [5, 39].

Example: Forced Stuart-Landau Oscillator. In this contribution we consider as an example the perturbed Stuart-Landau oscillator (SL)

$$\dot{a} = (\mu + i\nu)a - (1 + i\alpha)a|a|^2 + i\varepsilon P(t), \qquad P(t) = \cos(r\omega t) \tag{12.3}$$

where $a(t) := R(t)\exp[i\phi(t)]$ is the complex amplitude. Parameter μ determines the amplitude ($\sqrt{\mu}$) and stability of the limit cycles, α is the nonisochronicity parameter. It is easy to check that

$$\varphi(t) = \phi(t) - \alpha \ln[R(t)] \tag{12.4}$$

is the proper phase, rotating, independently of amplitude R, with uniform frequency $\omega = \nu - \mu\alpha$. The frequency of the forcing is $r\omega$, where parameter r is the ratio of the external frequency to the base frequency ω. In the first order in ε, the amplitude and the phase dynamics read

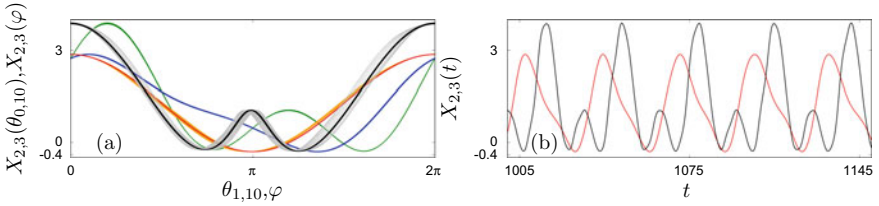

Fig. 12.1 Panel **a**: Observables X_2 (blue points) and X_3 (green points) as functions of the true phase φ. The fact that these sets are not distiguishable from a line demonstrates validity of the phase description for the SL oscillator (i.e. the amplitude modulation is indeed small). The same observables as functions of the first protophase θ_1 are not lines but broad sets (orange points for $X_2(\theta_1)$ and grey points for $X_3(\theta_1)$). The same observables become good function of the protophase θ_{10} after 10-th iteration of our procedure (red and black points, corerspondingly). Panel **b**: Time series for observables $X_{2,3}(t)$ (red,black). Simulation parameters are $\mu = 8, \alpha = 0.1, \nu = 1, \varepsilon = 0.1$ and $r = 1.8$ (for $X_2(t)$) and $r = 5.6$ (for $X_3(t)$). In this scale, small amplitude and phase modulations are hardly seen

$$\begin{aligned} \dot{R} &= R(\mu - R^2) + \varepsilon P(t)\sin(\varphi), \\ \dot{\varphi} &= \omega + \varepsilon\mu^{-1/2}(\cos(\varphi) - \alpha\sin(\varphi))P(t). \end{aligned} \tag{12.5}$$

Here, the iPRC is

$$Z(\varphi) = (\cos(\varphi) - \alpha\sin(\varphi))\mu^{-1/2}. \tag{12.6}$$

One can see that for small ε the dynamics of the SL is nearly periodic, with small ($\sim \varepsilon$) amplitude and phase modulations. Below in this paper we will consider three different scalar observables of the SL dynamics: $X_1(t) = \mathrm{Re}[a(t)]$, $X_2(t) = 0.1(\mathrm{Im}[a])^2 + 0.2(\mathrm{Re}[a])^2 + 0.3\mathrm{Im}[a] + 0.4\mathrm{Re}[a]$, and $X_3(t) = X_2(t) + 0.3\mathrm{Re}[a]\mathrm{Im}[a]$. The observable X_1 is "simple", it is a pure cosine function of time for the autonomous SL oscillator. The observable X_2 is also relatively simple (with one maximum and minimum pro period), but not a pure cosine. The observable X_3 can be viewed as a *multi-component signal* [11], with two maxima and minima pro period. Snapshots of the time series of corresponding signals $X_{2,3}(t)$ are illustrated in Fig. 12.1b.

12.3 Phase Reconstruction and Iterative Hilbert Transform Embeddings

12.3.1 Waveform, Phase and Demodulation

In Sect. 12.2 we introduced the phase dynamics concept for weakly perturbed oscillators. It is based on the equations of the original oscillator's dynamics. In the context of

data analysis, one faces a problem of the phase dynamics reconstruction solely from the observations of a driven oscillator. From the time series of a scalar observable, one wants to reconstruct the phase dynamics equation (12.2).

The first assumption we make is that the phase modulation of the process observed is much stronger than the amplitude modulation. Although, according to the theory, amplitude perturbations appear already in the leading order $\sim \varepsilon$ (cf. Eq. (12.5)), these variations could be small if the stability of the limit cycle is strong. Indeed, like example Eq. (12.5) shows, perturbations of the amplitude are inverse proportional to the stability of the limit cycle $\sim \varepsilon/\mu$, and are additionally small for μ large. Thus, for the rest of this chapter we assume that the dynamical process under reconstruction is solely determined by the dynamics of the phase.

Generally, a time series emanates from an observable $X[\mathbf{y}(t)]$ of the systems dynamics. According to the assumption above, we neglect amplitude modulation which means that we assume $\mathbf{y} = \mathbf{y}_0$, so that the scalar signal observed is purely phase modulated

$$X(t) = X[\mathbf{y}_0(\varphi(t))] =: S(\varphi(t)). \tag{12.7}$$

Here a 2π-periodic function $S(\varphi) = X[\mathbf{y}_0(\varphi)]$ is unknown, we call it the waveform. The reconstruction problem for the signal $X(t)$ is that of finding the waveform $S(\varphi)$ and the phase $\varphi(t)$. In Fig. 12.1a, we illustrate these waveforms for the observables $X_{2,3}$ of the SL oscillator. Plotting $X_{2,3}$ as functions of φ with dots, one gets extremely narrow lines which indicate that for chosen large stability of the limit cycle the amplitude dynamics can be neglected and decomposition is possible. On the contrary, if the observed signals possess essential amplitude modulation, $X(\varphi)$ would look like a band. In that case the above representation (12.7) is not adequate.

We stress here that a decomposition into the waveform and the phase is not unique. Indeed, let us introduce a new monotonous "phase" $\theta(t)$ according to an arbitrary transformation

$$\theta = \Theta(\varphi), \quad \Theta(\varphi + 2\pi) = \Theta(\varphi) + 2\pi, \quad \Theta' > 0. \tag{12.8}$$

Then the signal can be represented as $X(t) = S(\Theta^{-1}(\theta)) = \tilde{S}(\theta)$ with a new waveform $\tilde{S} = S \circ \Theta^{-1}$. Variables $\theta(t)$ are called protophases [17, 18]. Examples for mappings Eq. (12.8) are depicted in Fig. 12.4. To see the difference between protophases and true phase $\varphi(t)$, let us consider the non-driven, non-modulated dynamics. Here the phase $\varphi(t)$ grows uniformly $\dot{\varphi} = \omega$, while the protophase $\theta(t)$ grows non-uniformly, as

$$\dot{\theta} = \Theta'(\varphi)\omega = \omega\Theta'(\Theta^{-1}(\theta)) = f(\theta). \tag{12.9}$$

However, having a protophase and the function $f(\theta)$ governing its dynamics, one can transform to the true phase $\varphi(t)$ by inverting relation (12.8):

$$\frac{d\varphi}{d\theta} = \frac{1}{\Theta'(\varphi)} = \frac{\omega}{f(\theta)}, \quad \varphi = \int_0^\theta \frac{\omega d\theta'}{f(\theta')}. \tag{12.10}$$

Note that Eq. (12.10) is well defined as by construction, $\dot{\theta} = f(\theta) > 0$. In the case one observes driven oscillations, one approximately estimates $f(\theta) = \langle\dot{\theta}\rangle$, see [18] for details.

According to the discussion above, one can perform the phase reconstruction of an observed signal $X(t)$ in two steps:
(i) Find a decomposition $X(t) = \tilde{S}(\theta(t))$ into a waveform and a protophase, satisfying conditions

$$\text{(I):}\ \forall t, \dot{\theta}(t) > 0, \qquad \text{(II):}\ \tilde{S}(\theta) = \tilde{S}(\theta + 2\pi). \tag{12.11}$$

(ii) Perform a transformation from a protophase to the phase, so that the latter grows on average uniformly in time

$$\text{(III):}\ \langle\dot{\varphi}\rangle = \text{const}. \tag{12.12}$$

Conditions [I, II] ensure that the reconstructed protophase is monotonous and 2π-periodic. Condition [III] selects the phase as a variable uniformly growing in time, in contrast to other protophases which according to (12.9) grow with a rate that is protophase-dependent (with 2π-periodicity). Below we discuss in details the methods allowing for accomplishing steps (i) and (ii).

12.3.2 *Embeddings, Hilbert Transform, and Phase-Amplitude Mixing*

The first task, a decomposition into a waveform and a protophase, is trivial, if two scalar observables $\{X(t) = X[\mathbf{y}_0(t)], Y(t) = Y[\mathbf{y}_0(t)]\}$ of the oscillator's dynamics are available (of course, these observables should be not fully dependent). In this case, on the $\{X, Y\}$ plane one observes a *closed* continuous curve, parametrized by the phase, and the trajectory rotates along this curve. Any parametrization of the curve, normalized by 2π, will then provide a protophase as a function of time. After this, one has only to accomplish the step (ii), i.e. to transform the protophase to the phase.

An intrinsically non-trivial problem appears, if only one scalar observable, $X(t)$, is available. The goal is to perform a two-dimensional embedding of the signal $X(t)$, by generating from it the second variable $Y(t)$. There exist several approaches for this task. The most popular ones are the delay-embedding $Y(t) = X(t - \tau)$ [16], the derivative embedding $Y(t) = \dot{X}(t)$ [32], and the Hilbert transform (HT) embedding $Y(t) = \hat{H}[X](t)$, where (on a finite interval $[t_0, t_m]$)

$$\hat{H}[X](t) := \frac{\text{p.v.}}{\pi} \int_{t_0}^{t_m} \frac{X(\tau)}{t - \tau} d\tau. \tag{12.13}$$

It is an observation of practice, that the latter approach based on the HT often gives the most stable results. A reason for this is that the HT produces minimal distortions to the signal's spectrum. Indeed, all the methods mentioned are linear transformations, which in Fourier space correspond to multiplications with factors $e^{i\Omega\tau}$, $i\Omega$, and $i\ \mathrm{sign}(\Omega)$, respectively. The factor for HT depends on frequency in a "minimal" way, and does not have, contrary to the delay embedding, a parameter. However, the HT provides only an approximate embedding, due to a mixing of phase and amplitude modulations [13].

Indeed, only for a non-modulated, i.e. for a purely periodic signal $X(t)$, the HT transform provides a periodic $Y(t)$, so that on the $\{X, Y\}$ plane one observes a perfect closed loop. If the signal $X(t)$ is phase-modulated, then on the $\{X, Y = \hat{H}[X(t)]\}$ plane one observes a non-closed trajectory (which only approximately can be considered as a loop), the width of the band gives the size of the appearing amplitude modulation (see Figs. 12.1a and 12.2). (Also if one has a purely amplitude-modulated signal, its HT will provide spurious phase modulation - but this is not relevant for our problem). It should be noted that the spurious amplitude modulation arises solely due to the spectral properties of the Hilbert transform, and is not related to the length of the observation data. Usually, already 20–30 observed periods suffice to overcome boundary effects. Instead, the spectral content of the phase modulation heavily influences the appearance of amplitude modulation, and hence the accuracy of reconstruction [12].

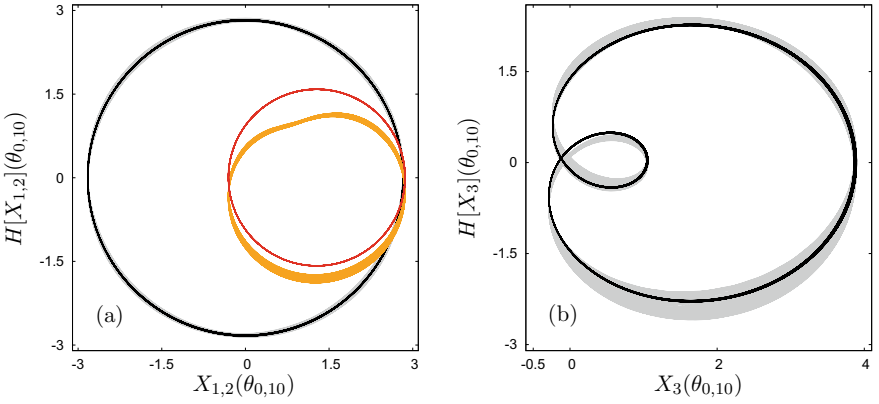

Fig. 12.2 IHTE for a periodically driven SL oscillator Eq. (12.3) with harmonic driving $P(t) = \cos(r\omega t)$. Parameters: $\mu = 8$, $\alpha = 0.1$, $\nu = 1$, $\varepsilon = 0.1$. In panel **a** observables $X_1(t)$ (for frequency ratio $r = 5.6$) and $X_2(t)$ (for $r = 1.8$) are used. Shown are the first step of the IHTE hierarchy in grey and orange, and step ten in black and red for X_1 and X_2, respectively. In panel **b** the observable $X_3(t)$ with $r = 5.6$ is used where grey corresponds to the first embedding and black corresponds to the embedding in step ten. Embeddings at the first iteration yield wide bands, which indicates for an "artificial" modulation of the amplitude, while at the 10th iteration the embeddings are nearly perfect lines, which means that the observed signals are nearly perfect phase modulated ones. Note that the embedding of X_1 has a circular shape, the embeddings of $X_{2,3}$ are distorted from a circle causing non-uniform protophases. In case of X_3, the embedding shows a loop (panel (**b**))

In the next section we describe a method to circumvent this problem by virtue of *iterated HT embeddings* (IHTE) [12], illustrating the procedure with different observables of the SL oscillator.

12.3.3 Iterated HT Embeddings

As discussed above, the HT embedding $\{X(t), \hat{H}[X(t)]\}$ although does not provide a closed looped line, allows one for an approximate determination of the protophase. To accomplish this, one needs to define a variable monotonously growing along the trajectory and gaining 2π at each approximate loop. A naive analytic-signal-based protophase $\arg(X + iY)$ would work only for cosine-like waveforms like $X_{1,2}$. Therefore we employ another definition of the protophase, based on the trajectory length [18]

$$L(t) = \int_0^t \sqrt{\dot{X}^2(\tau) + \dot{Y}^2(\tau)}d\tau. \tag{12.14}$$

This length grows monotonously also in the case when the embedding has loops (cf. Fig. 12.2), in which case the analytic-signal-based definition obviously fails.

Having calculated the length $L(t)$, we can transform it to a protophase by interpolation. For this, we define in the signal features which we attribute to the zero (modulo 2π) protophase, and define the corresponding time instants t_j. In the simplest case, one can define a protophase $\theta(t)$ on the interval (t_j, t_{j+1}) as a linear function of the length $\theta(t) = 2\pi j + 2\pi(L(t) - L(t_j))/(L(t_{j+1}) - L(t_j))$. However, such a protophase will be discontinuous in the first derivative. A better transformation is achieved via splines: one constructs a spline approximation for the function $\theta(L)$, provided one knows the values of this function at the signal features: $\theta(t_j) = 2\pi j$ at $L(t_j)$.

Constructed in this way, the protophase $\theta(t)$ is only approximate, because $X(\theta + 2\pi) \neq X(\theta)$. Visually, on the plane $\{X, \hat{H}[X]\}$ one observes a band instead of a single loop (see Fig. 12.2). Also, when X is plotted versus θ, one observes not a single-valued function, but a band (see Fig. 12.1a).

Recently, in Ref. [12], we proposed to use iterative Hilbert transform embeddings (IHTE) to improve the quality of the protophase definition above. Our idea is to perform subsequent Hilbert transforms based on the previously calculated protophases $\theta_n(t)$, where n denotes the step of iteration (see Fig. 12.3). Intuitively, the advantage of iterations can be understood as follows: The widely used first iteration already presents an approximation to the protophase, although not a perfect one. This means, that the function $X(\theta_1)$ still has modulation, but less than $X(t)$. Now, if we take θ_1 as a new time and again perform a demodulation by virtue of the Hilbert transform embedding, we expect $\theta_2(t)$ to be better than $\theta_1(t)$, etc. A detailed analysis performed in Ref. [12] shows that this procedure indeed converges to perfect demodulation.

In terms of iterations, the protophase $\theta(t)$ discussed above is the first iteration $\theta_1(t)$, while the time variable can be considered as the "zero" iteration $\theta_0(t)$. At each

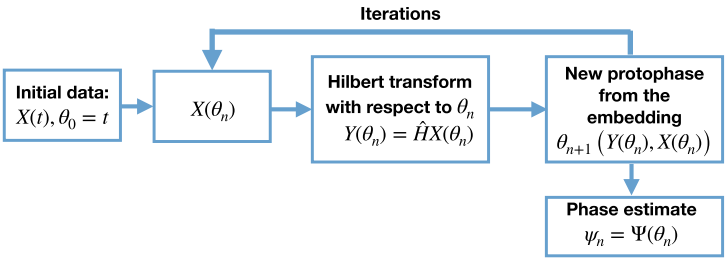

Fig. 12.3 Here we schematically explain the iterative Hilbert tranform embeddings. Typically only one iteration is performed, and the protophase $\theta_1(t)$ is used for further analysis. We show in this chapter, how the quality of the phase reconstruction improves with the iterative embeddings

iteration step we use the obtained protophase as a new "time" with respect to which the next HT is performed:

$$Y_{n+1}(\theta_n) = \hat{H}[X(\theta_n)] := \frac{\text{p.v.}}{\pi} \int_{\theta_n(t_0)}^{\theta_n(t_m)} \frac{X(\theta'_n)}{\theta_n - \theta'_n} d\theta'_n. \tag{12.15}$$

An implementation of this integral is given in [12]. Basically there are two challenges here: first, the integration has to be performed on a non-uniform grid and second, one has to take care of the singularity at $\theta'_n = \theta_n$.

The iteration process will be as follows (see Fig. 12.3):

1. Having $X(\theta_n) = X(t(\theta_n))$, we calculate $Y_{n+1}(\theta_n) = \hat{H}[X(\theta_n)]$ according to (12.15).
2. Next, we construct the embedding $\{X, Y_{n+1}\}$ and find the length $L(\theta_n)$ from (12.14).
3. After defining signal features, we calculate, using splines, the new protophase θ_{n+1} as a function of $L(\theta_n)$, which gives the new protophase θ_{n+1} as a function of the old one θ_n.

The steps 1–3 are repeated, starting from $\theta_0 = t$. After n iterations, we obtain a waveform and a protophase

$$\tilde{S}(\theta_n) = X(t(\theta_n)) \tag{12.16}$$

As has been demonstrated in Ref. [12], the procedure converges to a proper protophase, fulfilling conditions [I, II] above. For a purely phase modulated signal, at large n the errors (12.17) reach very small values limited by accuracy of integration. The convergence rate depends heavily on the complexity of the waveform and on the level and frequency of modulation, but typically at $\hat{n} \approx 10$ a good protophase is constructed.

Summarizing, the IHTE solve the problem of constructing a protophase $\theta(t) = \theta_{\hat{n}}(t)$ and the corresponding waveform $\tilde{S}(\theta)$ from a scalar phase-modulated signal $X(t)$; this protophase fulfills conditions (12.11)-[I, II]. Indeed, one observes in Fig. 12.4 that the first mapping $\Theta_1(\varphi)$ is not purely 2π-periodic (blue bands). Instead,

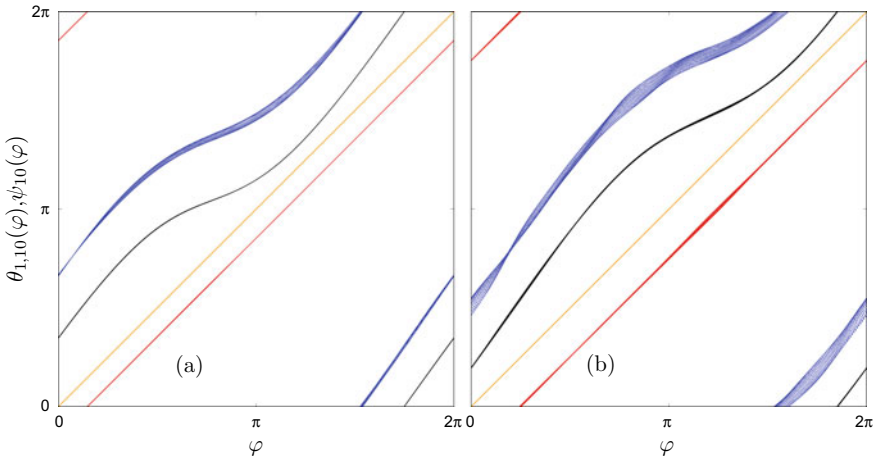

Fig. 12.4 Depicted are the phase-to-protophase maps Eq. (12.8) for $X_2[.]$ (panel **a**) and $X_3[.]$ (panel **b**) based on the embeddings shown in Fig. 12.2. Colours correspond to $\Theta_1(\varphi)$ (blue, this data form a rather wide band indicating that the protophase at the first iteration is not precise), $\Theta_{10}(\varphi)$ (black, this data forms a narrow line indicating for a good protophase reconstruction), $\psi_{10}(\varphi)$ (red, this narrow line is straight indicating for a good phase reconstruction). The orange line is the diagonal. For better visibility the curves are shifted vertically

after ten iterations, $\Theta_{10}(\varphi)$ effectively has become a line (black) indicating that a protophase is reconstructed. The same can be seen in Fig. 12.1a, where bands of values $X_{2,3}(\theta_1)$ are transformed to narrow lines $X_{2,3}(\theta_{10})$ after ten iterations.

As the final step in obtaining a close estimate $\psi(t)$ of the proper phase $\varphi(t)$, we have to perform the protophase-to-phase transformation, as described in Ref. [18]. The transformation is based on relation (12.10), where the Fourier components of the density of the protophase are estimated according to $F_k = t_m^{-1} \int_0^{t_m} \exp[-ik\theta(t)]\, dt$; these components are used to perform the transformation as $\psi = \theta + \sum_{k\neq 0} F_k (ik)^{-1} [\exp(ik\theta) - 1]$. Indeed, one observes in Fig. 12.4 (red lines) that $\psi(t)$ is, up to estimation errors, resembling the dynamics of $\varphi(t)$. However, we want to stress here that determination of the protophase-to-phase transformation is based on a statistical evaluation of the probability density of the protophase. Hence, in order to achieve a proper reconstructions with small distortions in the protophase-to-phase mapping, one needs long time series.

We can check for the similarity of $\theta_n(t)$ or $\psi_n(t)$ to the true phase $\varphi(t)$ by calculating a phase and a frequency error as the standard deviations

$$\mathrm{STD}_n^{\mathbf{q}} = \sqrt{\frac{1}{\hat{N}_1} \int_{t_{\min}}^{t_{\max}} [\mathbf{q}_n(\tau) - \varphi(\tau)]^2 d\tau} \qquad \mathrm{STD}_n^{\dot{\mathbf{q}}} = \sqrt{\frac{1}{\hat{N}_2} \int_{t_{\min}}^{t_{\max}} [\dot{\mathbf{q}}_n(\tau) - \dot{\varphi}(\tau)]^2 d\tau}$$

$$\hat{N}_1 = \int_{t_{\min}}^{t_{\max}} (\varphi(\tau) - \tilde{\omega}\tau)^2 d\tau \qquad \hat{N}_2 = \int_{t_{\min}}^{t_{\max}} [\dot{\varphi}(\tau) - \tilde{\omega}]^2 d\tau. \tag{12.17}$$

$\mathrm{STD}_n^{\mathbf{q},\dot{\mathbf{q}}}$ tend to zero only, if the reconstructed protophases and transformed protophases $\mathbf{q}_n = \{\theta_n(t), \psi_n(t)\}$ are close to the true phase $\varphi(t)$ of the system (see Eq.(12.4)). In the integration, we skip the outer ten percent at the beginning and at the end of the time series, to avoid boundary effects. Estimations of the instantaneous frequency $\varphi(t)$ and $\dot{\mathbf{q}}_n(t)$ are performed by a 12th order polynomial filter (Savitzky-Golay filter) with a window of 25 points and four times repetition [33] denoted as SG(12,25,4). Throughout the chapter we use a sampling rate of $dt = 0.01$, such that the smoothing window has a width of $dt = 0.25$, corresponding to roughly 11% of the fastest forcing period ($r = 14.3$). The estimated average growth rate $\tilde{\omega}$ is obtained by linear regression. Note that the normalization integral $\hat{N}_1$ is suitable for all phases where the average growth is linear.

12.4 Numerical Experiments

12.4.1 Deterministic Oscillations

Here we consider the SL system (12.3) with $\mu = 8$, $\alpha = 0.1$, $\nu = 1$. As the observables we explore functions $X_{1,2,3}[a(t)]$ defined above. The system is forced harmonically by $\varepsilon P(\eta) = \varepsilon \cos(\eta(t))$ with amplitude $\varepsilon = 0.1$. The external force phase is $\eta(t) = r\omega t$, for the explored range of driving frequencies $r\omega$ the SL operated in the asynchronous regime. We observe 100 periods with a time step of $dt = 0.01$.

In Fig. 12.6 the phase and the frequency errors according to Eq. (12.17) for the first 20 iteration steps are shown. While for slow modulations ($r < 1$), the reconstruction is already accurate in the first step, for fast forcing frequencies ($r > 1$) indeed several iterations are needed for precise reconstruction. The reason for this is that for high-frequency modulations iterative HT embeddings first shift high-frequency Fourier components of the phase modulation to lower frequencies, where they eventually disappear. This mechanism is closely related to the Bedrosian identities [40] and is explained in detail in [12]. For the reconstruction of phases in case of $X_{2,3}[a(t)]$, we have to calculate the transformed phase $\psi(t)$, because here the protophases deviate from uniform growth. The results show, that IHTE combined with the protophase-to-phase transformation provides proper phase reconstructions for the fairly stable limit cycle oscillator under study.

Figure 12.5 presents comparisons of the inferred modulation $u_n(t) := \psi_n(t) - \tilde{\omega}t$ with the true one $q(t) = \varphi - \omega t$, and of the inferred instantaneous frequencies $\dot{\theta}_n(t)/\dot{\psi}_n(t)$ with $\dot{\varphi}$, for a quite fast external force $r = 5.6$ (black bold dots in Fig. 12.6). While the first iterate is by far not accurate, iterations provide the reconstructed estimation of the phases $\psi_{20}(t)$ which is very close to $\varphi(t)$.

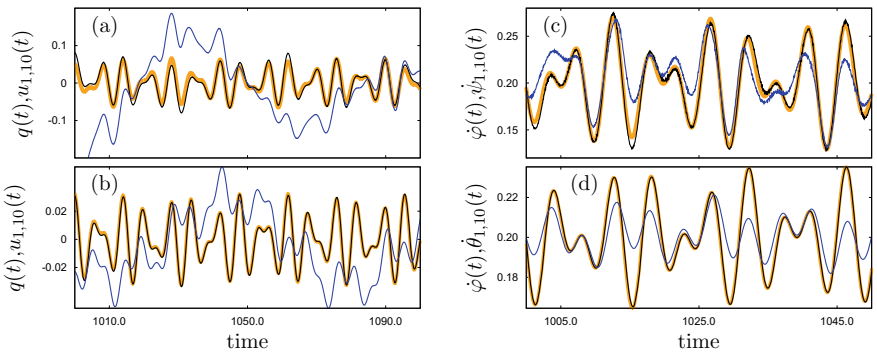

Fig. 12.5 Comparison of true modulation $q(t)$ and of true instantaneous frequency $\dot{\varphi}$ (orange) with the corresponding iteration results $u_n(t)$ in the first step (blue) and in the 10th step (black) for the observables $X_1(t)$ (b, d) and $X_3(t)$ (a, c). Parameters are $\mu = 8$, $\alpha = 0.1$, $\nu = 1$, $\varepsilon = 0.1$ and $r = 5.6$. For calculation of the derivative $\dot{\varphi}(t)$ we use a SG(12,25,4) filter

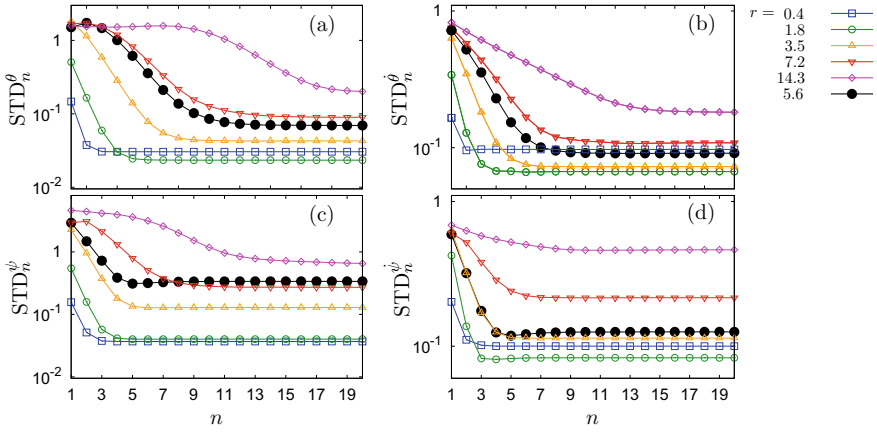

Fig. 12.6 Phase and frequency errors for observables $X_1(t)$ (a, b) and $X_2(t)$ (c, d) for different forcing frequencies $r\omega$. Also shown in (c, d black doted line) is the reconstruction error for $X_3(t)$, where the use of $L(t)$ for phase calculation is crucial. Slow modulations are essentially reconstructed in the first step while fast modulations need at least several iterations. With increased forcing frequency, $\theta_n(t)$ differs significantly from $\varphi(t)$ and the number of needed iterative steps grows

12.4.2 Reconstruction of the Phase Response Curve from Observation

Here, we present the advantage of using the IHTE for the reconstruction of the coupling functions and the iPRC. As an example we consider the SL oscillator with harmonic driving and parameters $r = 5.6$, $\mu = 8$, $\alpha = 0.1$, $\nu = 1$ and $\varepsilon = 0.1$ observed via variable $X_1[.]$. The coupling function is reconstructed by a kernel-density fit. Namely, we use a kernel $\mathbb{K}(x, y) = \exp[\kappa(\cos(x) + \cos(y) - 2)]$ and

$\kappa = 200$ to construct $\dot{\theta}(\varphi, \eta)$. We apply a simple iterative method described in [19]. After K iterative steps, the extracted coupling function $\tilde{Q}_{K,n}(\varphi, \eta) := \dot{\theta}_n(\varphi, \eta) - \tilde{\omega}$ is factorized into $\tilde{Z}_K(\varphi)$ and $\tilde{P}_K(\eta)$. In Fig. 12.8, the improvement due to IHTE is evident. We used $K = 30$ factorization steps and recover the actual coupling function with pretty high accuracy for different frequencies of forcing depicted in Fig. 12.7.

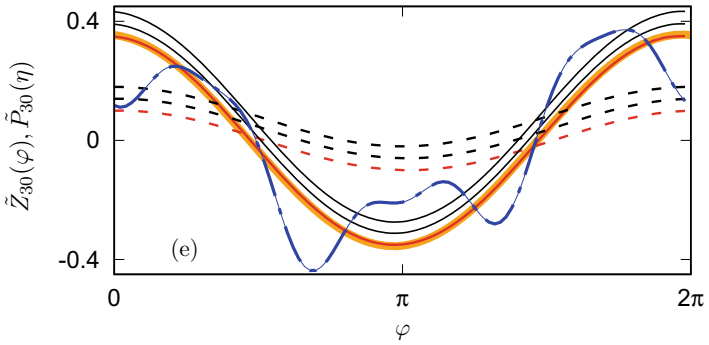

Fig. 12.7 The phase response curve $Z(\varphi)$ (orange). The blue unevenly dashed line depicts the estimation $\tilde{Z}_{30}(\varphi)$ based on $\theta_1(t)$. Also shown are the estimations $\tilde{Z}_{30}(\varphi)$ (solid line) and $\tilde{P}_{30}(\eta)$ (dashed line) based on $\theta_{10}(t)$ for $r = [0.06, 4.5, 5.6]$ (top to bottom). Red lines refer to the coupling functions Fig. 12.8

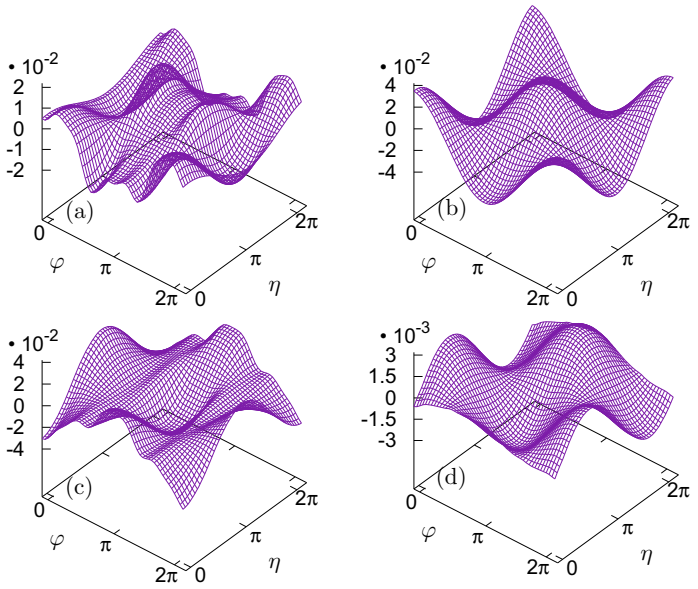

Fig. 12.8 Reconstructed coupling functions $\tilde{Q}_{30,1}(\varphi, \eta)$ (panel (a)) and $\tilde{Q}_{30,10}(\varphi, \eta)$ (panel (b)) based on $\theta_1(t)$ and $\theta_{10}(t)$, respectively. The reconstruction error for the first iteration $Q_{30,1}(\varphi, \eta) - Q(\varphi, \eta)$ is shown in panel (c), and for the 10th iteration $Q_{30,10}(\varphi, \eta) - Q(\varphi, \eta)$ in panel (d). Noteworthy, the vertical scale in panel (d) is more than ten times smaller than in panel (c)

12.4.3 Noisy Oscillations

In this section we discuss applicability of the described method to noisy signals. We assume that the SL oscillator is driven by an external force containing a deterministic and a stochastic (white noise) component

$$\varepsilon P(t) = \varepsilon \cos(\omega r t) + \xi(t), \qquad \langle \xi \rangle = 0, \langle \xi(t), \xi(t') \rangle = \sigma^2 \delta(t - t') \tag{12.18}$$

with $\mu = 8$, $\alpha = 0.1$, $\nu = 1$, $\varepsilon = 0.2$, $r = 5.6$ and different noise levels $\sigma = [0.1, 0.08, 0.06]$. We assume a "perfect" observation according to $X_1(t)$ (i.e., there is no observational noise). Due to the stochastic forcing, the signal's spectrum has infinite support. In the time domain, $X(t)$ contains an infinite amount of local maxima and minima which will cause infinitely many but small loops in the embedding (see Fig. 12.9b). Strictly speaking, we can not obtain phase from such a signal by calculating the length of the embedded curve, because the latter is a fractal curve.

Therefore, we can not deal with the raw signal $X(t)$. Instead, as a preprocessing, we smooth out fast small-scale fluctuations of $X(t)$ by a SG [4, 12, 25] filter, effectively cutting the spectrum of the signal at high frequencies. In such a setting with a finite-width spectrum, we expect that IHTE can improve the phase reconstruction.

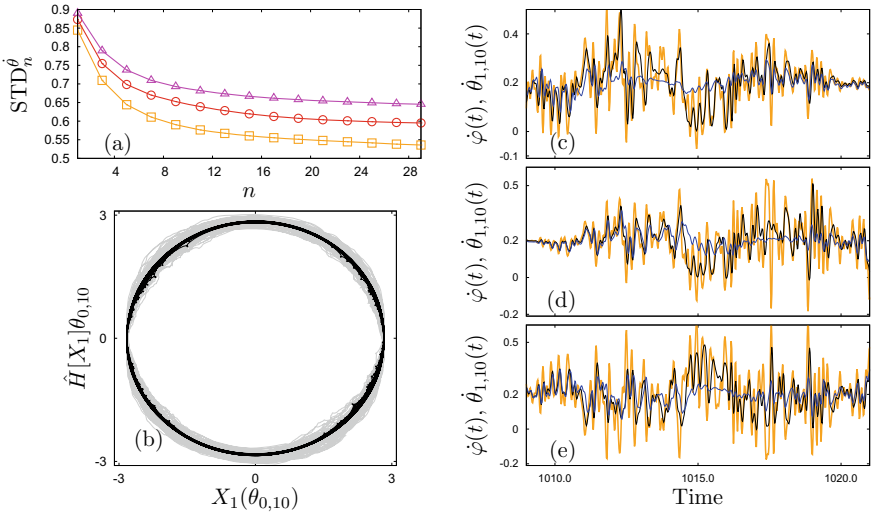

Fig. 12.9 Phase reconstruction for the SL system with $\mu = 8, \alpha = 0.1, \nu = 1, \varepsilon = 0.2$ and $r = 5.6$ and observable $X_1[.]$. Panel (a): the errors of frequency reconstruction for $\sigma = [0.06, 0.08, 0.1]$ (squares, circles, triangles). Panel (b): The first Hilbert embedding (grey) and the last embedding at 10th step (black). Note that the small scale loops as a result of the remaining noise influence in $X_1(t)$. Panels (c, d, e): Depicted are snapshots of the instantaneous frequency $\dot\varphi(t)$ (orange), and of the reconstructed frequencies $\dot\theta_1(t)$ (blue) and $\dot\theta_{10}(t)$ (black) for $\sigma = [0.06, 0.08, 0.1]$, respectively. Note that $\dot\varphi(t)$ can be negative as an effect of noise, while all reconstructions obey (12.11)-[I]

The results in this case have to be interpreted relative to the smoothing parameters which are chosen in such a way that they preserve essential local features of the dynamics. Indeed, we observe negative instantaneous frequencies $\varphi(t)$ pointing to the need of a high polynomial order of smoothing (see Fig. 12.9c, d, e). Also, the noise causes diffusion of phase (see Fig. 12.9).

From the viewpoint of phase extraction via embeddings, the white noise forcing represents a "worst case". On the contrary, in all situations where coloured noise with a bounded spectrum is present, we expect IHTE to be the more easily applicable. Depending on the spectral composition of noise, small-scale loops in the embedding may be not present at all, or may be eliminated with minimal filtering. If the noise has only relatively low-frequency component, the embedding will be relatively smooth, and no additional processing is needed.

Our method is restricted to the conditions (12.11). Since all of these conditions are not fulfilled in this example, the actual phase dynamics is only partly reconstructed, as can be seen also from Fig. 12.9a where the reconstruction error decay is much less pronounced than in Fig. 12.6. In view of this, the presented example can be considered as a proof of concept for IHTE of noisy signals. The method improves the estimation of the phase, as the examples of Fig. 12.9 show, by factor up to 2.

We add the following preprocessing to IHTE:

1. Given $X(t)$, apply a high-order SG-filter making the signal smooth with a large number of inflection points.
2. Next, smooth $\varphi(t)$ by the same SG-filter.
3. Proceed signal $X(t)$ with IHTE as described in Sect. 12.3.3.

12.5 Conclusion and Open Problems

In summary, the IHTE approach solves the problem of phase demodulation for purely phase modulated signals. Here, we present results for a dynamical system, where the amplitude dynamics is also present and linked to the dynamics of $\varphi(t)$. We have demonstrated that IHTE indeed provides a good reconstruction of the phase dynamics, if the amplitude variations are relatively small (see Fig. 12.4, 12.6, 12.5). We show that iterations drastically improve the reconstruction of the phase, in comparison to the previously employed approach based on a single Hilbert transform (see Fig. 12.5) and $Z(\varphi)$ (see Fig. 12.8). However, the analysis of the performance of IHTE in the case of larger amplitude variations is a question to be discussed in the future.

An important issue in the phase reconstruction is the protophase-to-phase transformation. It is particularly relevant for generic observables like $X_3[.]$, with complex waveforms. While handling such observables in the framework of IHTE does not state a problem, influence of amplitude variations may depend drastically on the complexity of the waveform. It should be stressed here, that while construction of the protophase via IHTE is almost exact, the protophase-to-phase transformation is

based on some assumption about the dynamics, which typically are only approximately fulfilled. This topic certainly deserves further studies.

Biological systems are noisy. We have given an example here, where IHTE also improves the reconstruction of the phase in presence of fluctuations (see Fig. 12.9). However, the very concept of a monotonously growing phase should be reconsidered for noisy signals. Here we largely avoided problems by smoothing the observed signal, but in this approach some features of the modulation might be lost.

Acknowledgements Both authors thank Aneta Stefanovska and Peter McClintock for the kind invitation to contribute to this interdisciplinary work. Erik Gengel thanks the Friedrich-Ebert-Stiftung for financial support. This paper was supported by the RSF grant 17-12-01534. The analysis in Sec. 3.3 was supported by the Laboratory of Dynamical Systems and Applications NRU HSE, of the Russian Ministry of Science and Higher Education (Grant No. 075-15-2019-1931).

References

1. A. Bahraminasab, F. Ghasemi, A. Stefanovska, P.V.E. McClintock, H. Kantz, Direction of coupling from phases of interacting oscillators: a permutation information approach. Phys. Rev. Lett. **100**, 084101 (2008)
2. H. Balzter, N.J. Tate, J. Kaduk, D. Harper, S. Page, R. Morrison, M. Muskulus, P. Jones, Multi-scale entropy analysis as a method for time-series analysis of climate data. Climate **3**(1), 227–240 (2015)
3. D. Benitez, P. Gaydecki, A. Zaidi, A. Fitzpatrick, The use of the Hilbert transform in ECG signal analysis. Comput. Biol. Med. **31**(5), 399–406 (2001)
4. K.A. Blaha, A. Pikovsky, M. Rosenblum, M.T. Clark, C.G. Rusin, J.L. Hudson, Reconstruction of two-dimensional phase dynamics from experiments on coupled oscillators. Phys. Rev. E **84**(4), 046201 (2011)
5. E. Brown, J. Moehlis, P. Holmes, On the phase reduction and response dynamics of neural oscillator populations. Neural Comput. **16**(4), 673–715 (2004)
6. S.L. Brunton, J.N. Kutz, *Data-Driven Science and Engineering: Machine Learning, Dynamical Systems, and Control* (Cambridge University Press, 2019)
7. R. Cestnik, M. Rosenblum, Reconstructing networks of pulse-coupled oscillators from spike trains. Phys. Rev. E **96**(1), 012209 (2017)
8. R. Chestnik, M. Rosenblum, Inferring the phase response curve from observation of a continuously perturbed oscillator. Sci. Rep. **8**(1), 13606 (2018)
9. L. Cimponeriu, M. Rosenblum, A. Pikovsky, Estimation of delay in coupling from time series. Phys. Rev. E **70**, 046213 (2004)
10. L. Cohen, P. Loughlin, D. Vakman, On an ambiguity in the definition of the amplitude and phase of a signal. Sig. Process. **79**(3), 301–307 (1999)
11. M. Feldman, *Hilbert Transform Applications in Mechanical Vibration* (Wiley, 2011)
12. E. Gengel, A. Pikovsky, Phase demodulation with iterative Hilbert transform embeddings. Sig. Process. **165**, 115–127 (2019)
13. R. Guevara Erra, J.L. Perez Velazquez, M. Rosenblum, Neural synchronization from the perspective of non-linear dynamics. Front. Comput. Neurosci. **11**, 98 (2017)
14. N.-H. Holstein-Rathlou, K.-P. Yip, O.V. Sosnovtseva, E. Mosekilde, Synchronization phenomena in nephron–nephron interaction. Chaos: Interdiscip. J. Nonlinear Sci. **11**(2), 417–426 (2001)
15. N. Jajcay, S. Kravtsov, G. Sugihara, A.A. Tsonis, M. Paluš, Synchronization and causality across time scales in El Niño Southern Oscillation. NPJ Clim. Atmos. Sci. **1**(1), 1–8 (2018)

16. H. Kim, R. Eykholt, J. Salas, Nonlinear dynamics, delay times, and embedding windows. Phys. D **127**(1–2), 48–60 (1999)
17. B. Kralemann, L. Cimponeriu, M. Rosenblum, A. Pikovsky, R. Mrowka, Uncovering interaction of coupled oscillators from data. Phys. Rev. E **76**(5 Pt 2), 055201 (2007)
18. B. Kralemann, L. Cimponeriu, M. Rosenblum, A. Pikovsky, R. Mrowka, Phase dynamics of coupled oscillators reconstructed from data. Phys. Rev. E **77**(6), 066205 (2008)
19. B. Kralemann, M. Frühwirth, A. Pikovsky, M. Rosenblum, T. Kenner, J. Schaefer, M. Moser, In vivo cardiac phase response curve elucidates human respiratory heart rate variability. Nat. Commun. **4**, 2418 (2013)
20. B. Kralemann, A. Pikovsky, M. Rosenblum, Reconstructing phase dynamics of oscillator networks. Chaos **21**(2), 025104 (2011)
21. C. Letellier, J. Maquet, L. Le Sceller, G. Gouesbet, L. Aguirre, On the non-equivalence of observables in phase-space reconstructions from recorded time series. J. Phys. A: Math. Gen. **31**(39), 7913 (1998)
22. D. Li, X. Li, Z. Liang, L.J. Voss, J.W. Sleigh, Multiscale permutation entropy analysis of EEG recordings during sevoflurane anesthesia. J. Neural Eng. **7**(4), 046010 (2010)
23. M. Paluš, Multiscale atmospheric dynamics: cross-frequency phase-amplitude coupling in the air temperature. Phys. Rev. Lett. **112**(7), 078702 (2014)
24. M. Paluš, A. Stefanovska, Direction of coupling from phases of interacting oscillators: An information-theoretic approach. Phys. Rev. E **67**, 055201 (2003)
25. Z. Peng, W.T. Peter, F. Chu, An improved Hilbert-Huang transform and its application in vibration signal analysis. J. Sound Vib. **286**(1–2), 187–205 (2005)
26. B. Pietras, A. Daffertshofer, Network dynamics of coupled oscillators and phase reduction techniques. Phys. Rep. (2019)
27. A. Pikovsky, M. Rosenblum, J. Kurths, *Synchronization: A Universal Concept in Nonlinear Sciences* (Cambridge University Press, 2001)
28. T. Rings, K. Lehnertz, Distinguishing between direct and indirect directional couplings in large oscillator networks: partial or non-partial phase analyses? Chaos: Interdiscip. J. Nonlinear Sci. **26**(9), 093106 (2016)
29. M. Rosenblum, L. Cimponeriu, A. Pikovsky, Coupled oscillators approach in analysis of physiological data. Conf. Proc. IEEE Eng. Med. Biol. Soc. **1**, 441–4 (2006)
30. M. Rosenblum, A. Pikovsky, Detecting direction of coupling in interacting oscillators. Phys. Rev. E **64**(4), 045202(R) (2001)
31. M. Rosenblum, A. Pikovsky, Synchronization: from pendulum clocks to chaotic lasers and chemical oscillators. Contemp. Phys. **44**(5), 401–416 (2003)
32. T. Sauer, J.A. Yorke, M. Casdagli, Embedology. J. Stat. Phys. **65**(3–4), 579–616 (1991)
33. A. Savitzky, M.J. Golay, Smoothing and differentiation of data by simplified least squares procedures. Anal. Chem. **36**(8), 1627–1639 (1964)
34. A. Schlemmer, S. Berg, T. Lilienkamp, S. Luther, U. Parlitz, Spatiotemporal permutation entropy as a measure for complexity of cardiac arrhythmia. Front. Phys. **6**, 39 (2018)
35. T. Stankovski, T. Pereira, P.V.E. McClintock, A. Stefanovska, Coupling functions: universal insights into dynamical interaction mechanisms. Rev. Mod. Phys. **89**, 045001 (2017)
36. T. Stankovski, S. Petkoski, J. Raeder, A.F. Smith, P.V. McClintock, A. Stefanovska, Alterations in the coupling functions between cortical and cardio-respiratory oscillations due to anaesthesia with propofol and sevoflurane. Philos. Trans. R. Soc. A: Math., Phys. Eng. Sci. **374**(2067), 20150186 (2016)
37. Ç. Topçu, M. Frühwirth, M. Moser, M. Rosenblum, A. Pikovsky, Disentangling respiratory sinus arrhythmia in heart rate variability records. Physiol. Meas. **39**(5), 054002 (2018)
38. A.B. Tort, R. Komorowski, H. Eichenbaum, N. Kopell, Measuring phase-amplitude coupling between neuronal oscillations of different frequencies. J. Neurophysiol. **104**(2), 1195–1210 (2010)
39. A.T. Winfree, *The Geometry of Biological Time*, vol. 12 (Springer Science & Business Media, 2001)

40. Y. Xu, D. Yan, The Bedrosian identity for the Hilbert transform of product functions. Proc. Am. Math. Soc. **134**(9), 2719–2728 (2006)
41. E. Yeung, S. Kundu, N. Hodas,Learning deep neural network representations for Koopman operators of nonlinear dynamical systems, in *2019 American Control Conference (ACC)* (IEEE, 2019), pp. 4832–4839
42. H. Yu, F. Li, T. Wu, R. Li, L. Yao, C. Wang, X. Wu, Functional brain abnormalities in major depressive disorder using the Hilbert-Huang transform. Brain Imaging Behav. **12**(6), 1556–1568 (2018)
43. D.A. Zappalà, M. Barreiro, C. Masoller, Uncovering temporal regularity in atmospheric dynamics through Hilbert phase analysis. Chaos: Interdiscip. J. Nonlinear Sci. **29**(5), 051101 (2019)